X International Conference on Computational Methods in Marine Engineering
MARINE 2023
J. García-Espinosa, L. González, J.E. Gutiérrez & B. Serván-Camas (Eds)

Towards Reliable Performance Predictions for Stommel's Perpetual Salt Fountain

Jost Kemper[1*], Jan Mense[†1], Kai Graf[1], Jörn Kröger[1] and Ulf Riebesell[†]

[1] Institute for Naval Architecture and Maritime Engineering, University of Applied Sciences Kiel, Grenzstraße 3, 24149 Kiel, Germany, web page: http://www.fh-kiel.de

[†] Biological Oceanography , GEOMAR Helmholtz Centre for Ocean Research Kiel, Düsternbrooker Weg 20, 24105 Kiel, Germany, web page: http://www.geomar.de

[*] Corresponding author: Jost Kemper, jost.kemper@fh-kiel.de

ABSTRACT

Artificial Upwelling (AU) of nutrient-rich Deep Ocean Water (DOW) to the ocean's sunlit surface layer is currently being investigated as a way of increasing the ecosystem productivity and enhancing the natural CO2 uptake of the ocean. AU is thus considered a marine Carbon Dioxide Removal (CDR) option (GESAMP, 2019) in addition to its potential in the context of open ocean fish and macroalgae farming (Kirke, 2003; Wu *et al.*, 2023). A promising technical concept for AU was described by the oceanographer Stommel *et al.* (1956). Stommel proposed that the counteracting effects of typical open ocean temperature and salinity depth profiles on density can be utilized to drive a self-sustaining upwelling flow in a vertical ocean pipe. He termed this effect the "perpetual salt fountain". Despite several research efforts, none of the previous studies were able to reliably predict or demonstrate the potential of Stommel Upwelling Pipes (SUP)s. The growing interest in AU in light of current CDR research poses the need for reliable performance prediction methods and further development of Stommel's concept. To fill this gap, two models have been developed in the present work. A Reynolds-Averaged Navier-Stokes (RANS) model and a one-dimensional numerical model. While the RANS model enables detailed modeling of the heat transfer and flow phenomena, the one-dimensional numerical model allows for fast evaluation of simplified geometries for optimization and large-scale studies. This twofold approach allows for effective performance predictions while ensuring good reliability of the results. The present work shows the results of a number of studies, performed for different geometries and environmental conditions. The results of both models are compared and analyzed, and the respective potential is demonstrated. The presented results provide insight into some key aspects of the performance of SUPs and their potential for AU.

Keywords: Artificial Upwelling; Perpetual Salt Fountain; Open-Ocean Aquaculture; Macroalgae Farming; Carbon Dioxide Removal (CDR); Computational Fluid Dynamics (CFD); OpenFOAM, Heat Transfer; Buoyancy-Affected Flow

NOMENCLATURE

General

P	pressure [N/m²]
Q	volumetric flow rate [L/s]
S_A	absolute salinity [g/kg]
Θ	conservative temperature [°C]
ρ	density [kg/m³]

RANS model

D	diffusivity of Salinity [m²/s]
$\boldsymbol{g}$	gravity vector [m/s²]
$\boldsymbol{I}$	unit matrix [-]
k	turbulent kinetic energy [m²/s²]
p^*_{rgh}	modified kinematic pressure $= \frac{1}{\rho_0}\left(\overline{P} - \rho \boldsymbol{g}\cdot\boldsymbol{r}\right) + \frac{2}{3}k$ [m²/s²]
$\boldsymbol{r}$	position vector w. r. t. water surface [m]
$\boldsymbol{S}$	strain rate tensor $= \frac{1}{2}\left(\nabla\overline{\boldsymbol{u}} + (\nabla\overline{\boldsymbol{u}})^T\right)$ [1/s]
t	time [s]
$\boldsymbol{u}$	velocity vector [m/s]
λ	thermal diffusivity [m²/s]
ν	kinematic viscosity [m²/s]
$\boldsymbol{\tau}^*$	deviatoric part of kinematic Reynolds stress tensor [m²/s²]

Subscripts

ϕ_0	constant reference quantity
ϕ_e	effective quantity $= \phi + \phi_t$
ϕ_t	quantity modeling turbulence effects

Superscripts

$\overline{\phi}$	Reynolds-averaged quantity
$\boldsymbol{\phi}^T$	transpose of tensor $\boldsymbol{\phi}$

1D model

A_c	pipe cross sectional area [m²]
c_f	Darcy pipe friction factor [-]
C_h	heat-transferring circumference [m]
c_p	specific heat capacity [J/kg K]
D	pipe diameter [m]
D_h	hydraulic pipe diameter [m]
g	gravity [m/s²]
h	convection heat transfer coefficient [W/m² s]
L	pipe length [m]
N_D	diameter-based Nusselt number $= \frac{hD}{\kappa}$ [-]
s	pipe wall thickness [m]
U	overall heat transfer coefficient across pipe wall [W/m² K]
w	pipe velocity [m/s]
z	vertical pipe coordinate (positive down) [m]
κ	thermal conductivity [W/m K]
$\Delta_r\Theta$	radial temperature difference [K]

Subscripts

ϕ_{av}	streamwise averaged quantity
ϕ_e	quantity in regards to the outer diameter of the inner pipe
ϕ_i	quantity in inner pipe
ϕ_{top}	quantity at upper pipe end
ϕ_o	quantity in outer pipe
ϕ_{ocean}	quantity in surrounding ocean
ϕ_{wall}	quantity of pipe wall material

1. INTRODUCTION

In the scientific community, a strong consensus exists on the fact that active removal of CO_2 from the atmosphere (CDR) is necessary to achieve net zero anthropogenic CO_2 emissions and limit global warming (IPCC, 2021). In current CDR proposals, the ocean plays an important role, with several marine CDR options currently being actively researched (GESAMP, 2019). Bringing nutrient-rich Deep Ocean Water (DOW) to the ocean's sunlit surface layer through a process called Artificial Upwelling (AU) can increase the productivity of ocean ecosystems, subsequently fostering CO_2 uptake. AU is thus considered as a standalone CDR option (Lovelock and Rapley, 2007; GESAMP, 2019) or in combination with other CDR measures, like open-ocean macroalgae mariculture and sinking (Wu *et al.*, 2023).

From a technical perspective, the task of providing nutrient-rich DOW for algal growth comes down to two main challenges, pumping the DOW to the surface and preventing it from sinking back down again, due to its high density. While several concepts for pumping the DOW to the surface have been proposed (Lovelock and Rapley, 2007; Liang and Peng, 2005; Stommel *et al.*, 1956), the challenge of keeping the DOW in the surface layer is still largely unresolved (Kirke, 2003; Kemper *et al.*, 2022; Fan *et al.*, 2015). A potential way of overcoming both challenges has been described by the oceanographer Stommel *et al.* (1956). In many ocean regions the surface waters have both, a higher temperature and a higher salinity than the DOW. With regard to density stratification, the effect of temperature predominates, so that the water column is stably stratified. The smaller salinity effect counteracts the temperature effect, thus reducing the stability of the water column. Stommel proposed to utilize these counteracting (stabilizing and destabilizing) effects for AU. If a vertical ocean pipe is filled with DOW (cold, low salinity) once, the water in the pipe will eventually be heated up by the surrounding ocean while the salinity difference persists, rendering the water in the pipe positively buoyant (i.e. lighter than the surrounding water). Stommel thus postulated that an upwelling flow in a vertical pipe, once triggered would sustain itself without additional energy input. Stommel called this phenomenon the *perpetual salt fountain*. In the present work, all AU concepts which are based on Stommel's principle will be subsumed under the term Stommel Upwelling Pipe (SUP). It should be noted at this point, that a self sustaining downwelling flow can be achieved in the same manner, if the pipe is initially filled with surface water (warm, high salinity) instead of DOW. For AU, which is usually proposed for implementation in remote ocean regions and potentially harsh environments, Stommel's concept has a number of desirable features. Apart from the initial triggering of the flow, it does not require any external energy supply. Its structure is technologically simple and the upwelled DOW is already heated up when leaving the system at the surface and thus has less tendency to sink back to depth.

A number of studies have been carried out in order to demonstrate and quantify the potential of Stommel's concept. In 1958, Groves published first flow rate calculations for SUP systems (Groves, 1958). Groves analyzed his results with respect to increased fish farming yields due to AU. He concluded that fertilization of fish farms by AU, using Stommel's concept, was not likely to be economically favorable over other fertilization options. Groves calculations were extended with respect to vertical heat conduction by Hinman (1966). Hinman found that vertical heat conduction had a negligible influence on the calculated flow rates. Yet, by investigating different ocean profiles and pipe geometries, he found significantly larger flow rates than Groves.
A new concept was introduced by Johnson and Decicco (1983). Based on the fact that Stommel's concept can be utilized for both, self sustaining up- and downwelling flow, Johnson and Decicco proposed a counterflow device where downwelling flow was realized in a large number of pipes running through an outer shell with upwelling flow.
As Johnson and Decicco point out, this device essentially mimics a shell-and-tube counterflow heat exchanger. From some optimization studies, using a simplified model, they concluded that the concept should be further studied in the context of mariculture farms. More recently, further research on SUP systems has been performed in the context of a Japanese mariculture project proposal (Maruyama *et al.*, 2004; Zhang *et al.*, 2004; Tsubaki *et al.*, 2007; Sato *et al.*, 2007; Maruyama *et al.*, 2011). Three field experiments with a single flexible 280 m pipe were carried out. The results were extended with calculations from a Reynolds-Averaged Navier-Stokes (RANS) model. The flow rates obtained in the field experiments, despite being of limited magnitude, strongly exceeded the model predictions. The disagreement of the model results with the experiments was attributed to the fact that turbulence was measured in the experiments while the model predicted laminar flow (Zhang *et al.*, 2004). Zhang *et al.* (2006) explained the measured turbulence based on the movement of the pipe due to surface waves.

The current lack of reliable performance predictions for SUPs can clearly be seen from this brief literature review. While only minor flow rates have been experimentally shown to date, mathematical and numerical models have not been validated in a way that would support their general predictive capabilities. Reliable modeling is needed to evaluate the potential of SUPs for AU. It thus represents a necessary milestone in the research and development around AU-based CDR approaches.

In the present work two new numerical methods are presented which are applicable to a wide range of SUP systems. The first method solves a set of pipe flow equations, based on a one-dimensional spatial discretization of the pipe. This method will be termed the one-dimensional method in the following. The second method solves the RANS equations, based on a two- or three-dimensional finite volume discretization. This method will further be referred to as the RANS method. While the one-dimensional method is capable of studying large experimental matrices within a short time, the RANS method offers full flexibility with respect to the device geometry. The latter also provides a more detailed insight into relevant flow features, like the velocity and temperature profiles across the pipe diameter, and generally implements a lower level of empirical assumptions. In the absence of full scale validation data,[1] the twofold approach at least allows for code-to-code validation between the results of the two models, thereby providing a first step towards reliable performance predictions for SUP systems.

The remainder of this paper will be structured as follows. The two methods will be described in detail in Section 2. In Section 3, first a description of relevant device geometries and deployment regions will be given. The results from both models will then be compared and discussed for a number of single SUP and counterflow SUP cases. Finally, results from a study on shell-and-tube type SUPs will be presented, before finishing with conclusions and recommended future work in Section 4.

2. NUMERICAL METHOD

2.1 RANS Method

The RANS method used in this work is similar to the method described in Kemper *et al.* (2022), however, instead of solving the full compressible set of RANS equations, the oceanic Boussinesq approximation is made here. The oceanic Boussinesq approximation, as described by Young (2010), consists of three steps:

1. The exact density ρ in the momentum equation is replaced by a constant reference density ρ_0 everywhere but in the buoyancy term.
2. The incompressible continuity equation $\nabla \cdot \boldsymbol{u} = 0$ is used.
3. An equation of state (EOS) of the form $\rho = f\left(\overline{S_A}, \overline{\Theta}, P_0 + \rho_0 \boldsymbol{g} \cdot \boldsymbol{r}\right)$ is used, where $\overline{\Theta}$ is the conservative temperature of McDougall (2003), $\overline{S_A}$ is absolute salinity, P_0 is the reference pressure at the water surface, $\boldsymbol{g}$ is the gravitational acceleration vector and $\boldsymbol{r}$ is the position vector with respect to a reference position at the water surface, where P_0 is taken.

Note that in the equation of state the pressure is approximated as a linear hydrostatic pressure, based on the constant reference density. By using a full EOS (IOC *et al.*, 2010) , the oceanic Boussinesq set has a wider range of applicability, when compared to the standard Boussinesq set of RANS equations.

[1]The results of Maruyama *et al.* (2004) cannot be used for model validation, as these results are highly influenced by an effect they attribute to wave action on the pipe. Since the actual salt fountain effect is very small in the experiment it cannot be separated from the wave effect.

The oceanic Boussinesq set of RANS equations can be written as:

$$\begin{aligned}
\frac{\partial\left(\overline{\boldsymbol{u}}\right)}{\partial t}+\nabla\cdot\left(\overline{\boldsymbol{u}}\overline{\boldsymbol{u}}\right) =& \nabla\cdot\overline{\boldsymbol{\tau}_e^*}-\nabla\overline{p_{rgh}^*}+\left(\boldsymbol{g}\cdot\boldsymbol{r}\right)\nabla\frac{\rho}{\rho_0}\\
\nabla\cdot\overline{\boldsymbol{u}} =& 0\\
\frac{\partial\left(\overline{\Theta}\right)}{\partial t}+\nabla\cdot\left(\overline{\boldsymbol{u}}\overline{\Theta}\right) =& \nabla\cdot\left(\lambda_e\nabla\overline{\Theta}\right)\\
\frac{\partial\left(\overline{S_A}\right)}{\partial t}+\nabla\cdot\left(\overline{\boldsymbol{u}}\overline{S_A}\right) =& \nabla\cdot\left(D_e\nabla\overline{S_A}\right)\\
\rho =& f\left(\overline{S_A},\overline{\Theta},p_0+\rho_0\boldsymbol{g}\cdot\boldsymbol{r}\right)
\end{aligned} \tag{1}$$

In Equation (1) $\overline{\boldsymbol{u}}$ is the velocity vector, ρ and ρ_0 are density an reference density, respectively. Further, t is time, $\boldsymbol{g}$ is the gravitational acceleration vector and $\boldsymbol{r}$ is the position vector. The effective diffusivities of temperature and salinity are denoted as λ_e and D_e, respectively and include laminar diffusion and the modeling of turbulence effects. $\overline{\boldsymbol{\tau}_e^*}$ is the deviatoric part of the effective kinematic Reynolds stress tensor which is modeled based on the linear eddy viscosity hypothesis (Morrison, 2013, p. 850)

$$\overline{\boldsymbol{\tau}_e^*}=2\nu_e\overline{\boldsymbol{S}}-\frac{2}{3}\nu_e\left(\nabla\cdot\overline{\boldsymbol{u}}\right)\boldsymbol{I}\ , \tag{2}$$

where ν_e is the effective viscosity and $\overline{\boldsymbol{S}}$ is the mean strain rate tensor.[2] $\overline{p_{rgh}^*}$ in Equation (1) is the modified kinematic pressure, which is calculated from the static pressure as $\overline{p_{rgh}^*}=\frac{1}{\rho_0}\left(\overline{P}-\rho\boldsymbol{g}\cdot\boldsymbol{r}\right)+\frac{2}{3}k$, with k being the turbulent kinetic energy.

The Finite Volume Method (FVM) is used to represent the equation set (1) by a set of algebraic equations for a finite number of locations in space and time. The *OpenFOAM* framework is used for the implementation. The equation set is solved in a pressure based manner, using *OpenFOAMs SIMPLE* and *PIMPLE* algorithms for steady state and transient flow, respectively. The following schemes are used for the discretization of the equations: Linear interpolation is used to obtain cell face values from the cell-centred data. Gradients are discretized using the Gauss method with linear interpolation. For the convective terms, the second-order accurate *Gamma* scheme of Jasak *et al.* (1999) and Linear Upwind schemes are applied. For the temporal derivative, the first-order implicit *Euler* scheme is used. This is appropriate, since the results presented here generally have a stable final state, which is of more interest than the exact temporal development towards this state.

Menters k-ω SST turbulence model is used for all simulations within this work (Menter, 1994). This choice was made based on the widespread use of this model for similar applications and its ability to run as a low-Reynolds turbulence model i. e. without the use of empirical wall functions. The details of this two-equation turbulence model will not be described here, for brevity. Detailed descriptions of the k-ω SST turbulence model can be found in (Menter, 1994) and (Menter *et al.*, 2003).

2.2 One-Dimensional Method

In this section, a one-dimensional model for the SUP is derived. The calculation method is described in a generalized form, highlighting the slight differences between the counterflow and single SUPs methods.
The self-sustaining flow in a SUP is driven by the differences in weight between the water-columns

[2] See nomenclature for details.

inside and outside of the respective pipe i.e. by an imbalance in the hydrostatic pressure at the pipes bottom end. For a fully developed steady-state flow, a balance between the viscous pressure loss of the pipe flow and the driving hydrostatic pressure imbalance can be formulated

$$c_{f\,av}\frac{\rho_{av}}{2}\frac{w_{av}^2}{D_h}L = g\left|\left(\int_{z_{top}}^{z=z_{top}+L}\rho_{ocean}dz - \int_{z_{top}}^{z=z_{top}+L}\rho dz\right)\right| \ . \tag{3}$$

Here, w_{av} is the flow velocity, $c_{f\,av}$ is the Darcy pipe friction factor, D_h is the hydraulic pipe diameter, L is the pipe length, g is the gravitational acceleration, z is the depth (positive downwards), and ρ and ρ_{ocean} denote the density of the water inside the pipe and the far-field, respectively. Please note that all flow quantities represent a radial averaged value over the respective region, e.g. the pipe, and just vary along the streamwise (z) direction. The subscript ϕ_{av} denotes, that the respective quantities are derived at the streamwise averaged density in the pipe. The water density can be calculated from the EOS

$$\rho = f\left(S_A, \Theta, P\right) \ . \tag{4}$$

where Θ, S_A and P are conservative temperature, absolute salinity and pressure, respectively. The hydrostatic pressure can be used for P, which leaves S_A and Θ as independent parameters. For the ocean outside the pipe, these parameters are known functions of the depth z. Inside the pipe, S_A uniformly takes the value of the water entering the pipe at the inlet, while Θ has to be modelled.

A simple model for the temperature inside the SUP can be developed based on the balance between convective heat transfer along the pipe (i.e. in the z-direction) and conductive heat transfer through the pipe wall. The resulting ordinary differential equation for Θ reads

$$-A_c w c_p \rho\frac{\partial\Theta}{\partial z} + C_h U \Delta_r\Theta = 0 \ . \tag{5}$$

Here, A_c is the cross sectional area of the pipe ($\frac{\pi}{4}D^2$ for a circular pipe), C_h is the heat-transferring circumference (πD for a circular pipe) and c_p is the heat capacity of the seawater, while $\Delta_r\Theta$ is the radial temperature difference. U is the overall heat transfer coefficient, which incorporates the thermal resistance of the pipe wall as well as the influence of the convection inside and outside the pipes. $U_n = f\left(D_n\right)$ with D_n being an arbitrary diameter can be calculated as

$$U_n = \frac{1}{D_n\sum\left({}^{D_m}/_{h_m}\right)} \ . \tag{6}$$

$${}^{D_m}/_{h_m} = \begin{cases} \frac{1}{N_{D\,i}\kappa_i}, & \text{inner pipe} \\ \frac{1}{2\kappa_{wall}}\ln\left(\frac{D_e}{D_i}\right), & \text{pipe wall} \\ \frac{D_{h\,o}}{D_e N_{Dh\,o}\kappa_o}, & \text{outer pipe} \\ \frac{1}{N_{D\,e}\kappa_{ocean}}, & \text{ocean} \ . \end{cases} \tag{7}$$

In Equation (7), D_i and $D_e = D_i + 2s$ are the inside and outside diameter of the inner pipe, while $D_{h\,o}$ represents the hydraulic outer pipe diameter in a counterflow setup. The Nusselt numbers corresponding to the inner, inner external and hydraulic outer pipe diameter are denoted as $N_{D\,i}$, $N_{D\,e}$ and $N_{Dh\,o}$. While s and κ_{wall} are the thickness and thermal conductivity of the pipe wall, κ_i, κ_o and κ_{ocean} are the thermal conductivities of the seawater within the inner pipe, outer pipe and the ocean, respectively. Please note that the heat transfer to the ocean was neglected for the counterflow setup. This may actually be a realistic assumption, considering that the outer shell will generally have to provide structural stability to the counterflow SUP system, such that the thickness of the inner pipes

can be minimized for lower thermal resistance. Although no extensive studies were performed in order to quantify the influence of outer pipe conductivitiy on the total upwelling and downwelling rates, the effect is estimated to be small.

In the proposed model, the Nusselt number N_D and the pipe friction coefficient c_f are the main empirical coefficients. Their correct determination has significant influence on the flow rates. A great number of correlations for N_D and c_f have been proposed in literature. While c_f was calculated using Morrisons formulation for smooth pipes over the entire Reynolds number range (Morrison, 2013, p. 533) with the Reynolds number correction proposed by Shah and Sekulić (2003, p. 487) for the outer pipe, the calculation of N_D required a more cautious handling. The natural convection N_D was calculated following the recommendations of Thess and Kaiser (2018b, p. 5, 6) while the forced convection N_D was calculated following the recommendations of Gnielinski (2018a) for the inner and (Gnielinski, 2018b) for the outer pipe. Natural and forced N_D where blended cubically following Thess and Kaiser (2018a, p. 7) and corrected for radially varying fluid properties following Shah and Sekulić (2003, p. 531). N_D for the ocean was calculated using the formulae of Churchill and Chu (Incropera *et al.*, 2013, p. 605) along with the correction of Popiel *et al.* (2007, p. 611) for vertical slender cylinders (fitted to the numerical results of Cebeci (1974)).

To find a solution for the proposed model for a given pipe geometry and a given ocean profile (i. e. Θ and S_A), the pipe is discretized in the axial direction and an iterative process is employed which solves Equations (5) and (3) within a given tolerance. For the counterflow setup $\Delta_r\Theta = f\left(\Theta_i(z), \Theta_o(z)\right)$, so Equation (5) has to be solved in a coupled manner for the inner and outer pipe. This can be done using a collocation algorithm for boundary value problems. For a single pipe setup $\Delta_r\Theta = f\left(\Theta_i(z), \Theta_{ocean}(z)\right)$ and Equation (5) can be efficiently solved for Θ, using the Runge-Kutta (Burg *et al.*, 2013, p. 55f) method. Equation (3) can be rearranged to obtain a solution for w (which can again feed into Equation (5)). Here, the following iterative solution process is used:

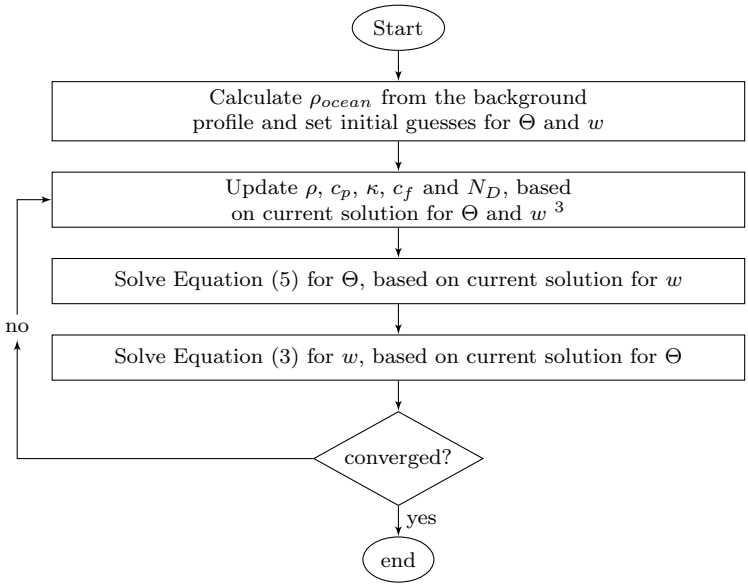

Figure 1: Flow diagram one-dimensional method

[3]In this work, the TEOS-10 equation of state for seawater IOC *et al.* (2010) is used for ρ and c_p, while *kappa* was calculated using the method of Jamieson and Tudhope (1970).

A number of important details about this set of equations for SUP systems have to be pointed out: First, it has to be noted that the heat balance described in Equation (5) is a mere balance of vertical convection and horizontal conduction. A set of equations including vertical conduction has been described by Hinman (1966), who concluded that the effect on the flow rate was negligible. Further, potential and latent energy were not considered in Equation (5) as their effect on the flow is expected to be negligible.
Although the presented equations and methods can be used independently of the SUP setup, the calculation of N_D and c_f is strongly dependent on the geometry. Nevertheless, using $D_h = \frac{4A_c}{C}$ with C as wetted perimeter, the above methodology for determining N_D and c_f can also be used to calculate configurations with multiple inner pipes. This will be further discussed in Section 3.5.

3. RESULTS AND DISCUSSION

In this section, results from SUP studies carried out with both models are described and discussed. First, a benchmark geometry for a single and counterflow SUP is defined and the RANS calculation setup is described. Subsequently, after a brief discussion on relevant ocean conditions, studies on different deployment regions and different pipe diameters will be presented, each time comparing both single and counterflow SUPs and the results from both models described in Section 2. Finally, a study on shell-and-tube type SUPs will be presented, providing some insight into the scaling of these devices.

3.1 Pipe Geometry and Calculation Setup

Single and counterflow SUPs represent the two main types of SUPs studied in this work. For simplicity, a benchmark geometry for these SUP types is defined here which describes all main particulars relevant for the calculations. A corresponding shell-and-tube type SUP geometry will be derived in Section 3.5. The benchmark geometries are depicted in Figure 2.

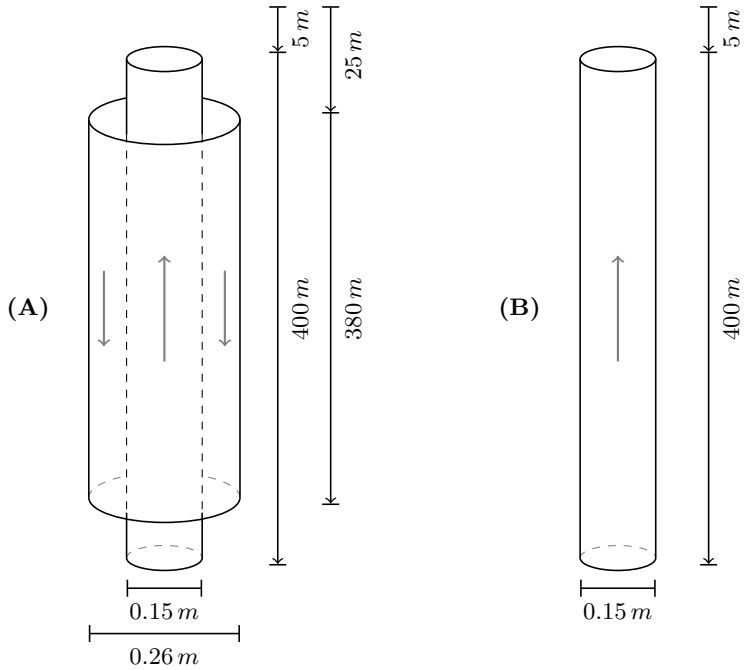

Figure 2: Stommel-pipe system concepts and main dimensions used in this study. (A) counterflow concept, (B) single pipe concept. All length dimensions are given with respect to the water surface.

As can be seen, both setups have a bottom depth of 400 m, a top depth of 5 m and a (inner) pipe diameter of 0.15 m. The outer pipe diameter of the counterflow SUP is chosen such that the inner-to-outer-pipe cross-sectional flow area ratio takes a value of 0.5. Thickness and thermal conductivity of the (inner) pipe wall were chosen such that a value of $2 \times 10^{-3}\,\mathrm{K\,m^2/W}$ for the thermal resistance $\frac{s}{\kappa_{wall}}$ is obtained. This is representative of a HDPE pipe with $s = 1\,\mathrm{mm}$ or a steel pipe with $s = 90\,\mathrm{mm}$. The outer pipe of the counterflow SUP is considered perfectly insulating as described in Section 2.2.

For the RANS model, several options are possible for the calculation setup. It generally seems advisable to exploit the axial symmetry of the system. The calculation thereby becomes two-dimensional, which greatly reduces the computational effort when compared to a full tree-dimensional calculation. The surrounding ocean around the pipe can either be included in the model, as done by Zhang *et al.* (2004), or represented by boundary conditions. In the context of this work both options have been tested and it was found that the results generally agreed very well, as will be shown in Section 3.3. The results presented here thus generally use the idealized setup without a resolved background ocean. The following boundary conditions are specified. All inlets of the pipes are total pressure inlets (i. e. the pressure is specified as the hydrostatic pressure from the background ocean minus $0.5\,|\boldsymbol{u}|^2$ while the velocity is calculated from the pressure equation). The transported scalar quantities (i. e. Θ, S_A and turbulence quantities) are specified based on the background ocean values. All outlets of the pipes are pressure outlets (i. e. the pressure is specified as the hydrostatic pressure from the background ocean and a Neumann boundary condition is applied for the velocity), where Neumann boundary conditions are applied for the transported scalar quantities. No-slip conditions are applied on all solid walls. For the counterflow SUP the outer pipe wall is adiabatic, while the inner pipe wall is implemented as a temperature baffle which accommodates for the appropriate heat transfer between the pipes. For the single SUP, the heat transfer with the background ocean is modeled, using a convective boundary condition at the pipe wall. This boundary condition sets Θ at the wall based on the background ocean value, taking into account the thermal resistance of the pipe wall and the assumed convection outside of the pipe. Here, the convection outside the pipe is calculated using the correlation of Churchill and Chu (1975).

Since both models described in Section 2 are solved numerically, it has to be ensured that the discretization is sufficiently fine. For the one-dimensional method the discretization is managed internally by the ordinary differential equation solver. For the RANS method discretization studies have been carried out to determine the appropriate mesh resolution. Based on these studies, a resolution of 25 cells across the pipe radius and 2500 cells across the pipe length was chosen, for which the discretization error in the upwelling velocity was estimated to be negligible.

3.2 Open ocean depth profiles

Salinity differences between the depths of a SUP's outlet and inlet can easily be identified as an important driver for the efficiency of SUP systems. Figure 3 shows the annual mean salinity difference between the sea surface and 400 m depth, based on WOA18 data (Boyer *et al.*, 2018) (mean over the years 1995 to 2018). Here, it can be seen that high salinity differences can almost exclusively be found in the subtropical ocean gyres. With relatively calm weather conditions, low seasonality, and low productivity, these regions are often seen as ideal regions for AU. If only areas with a salinity difference of $1.2\,\mathrm{g/kg}$ and above are considered, four confined regions are found, which correspond to the North Atlantic Gyre (NAG), the South Atlantic Gyre (SAG), as well as the North Pacific Gyre (NPG), and the South Pacific Gyre (SPG). Average annual depth profiles can now be derived as spatial average for each of these regions. Figure 4 shows these profiles along with seasonal (i. e. Spring, Summer, Autumn and Winter) mean profiles (over the years 1955 to 2018).

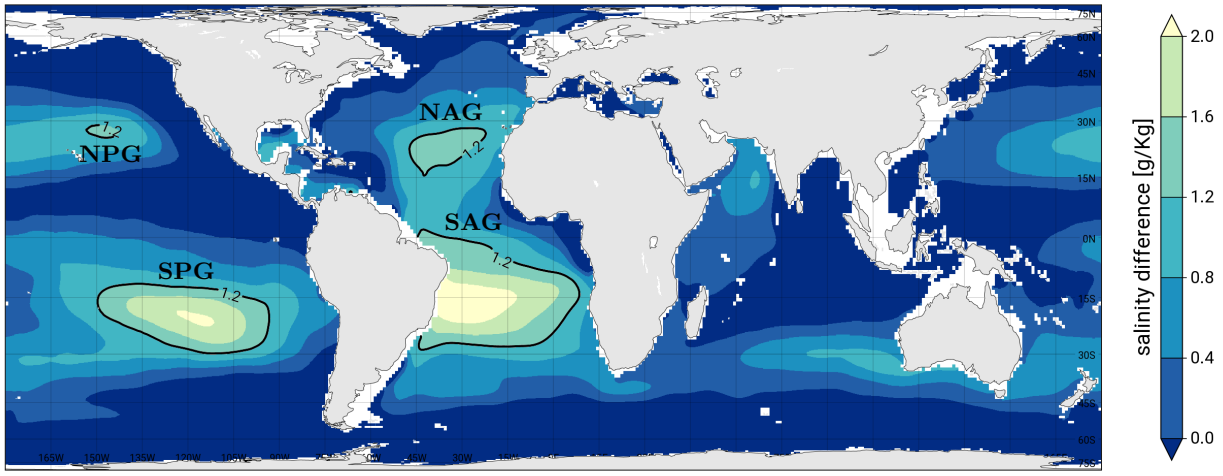

Figure 3: Annual mean S_A differences between surface and 400 m depth. Data taken from Boyer *et al.* (2018).

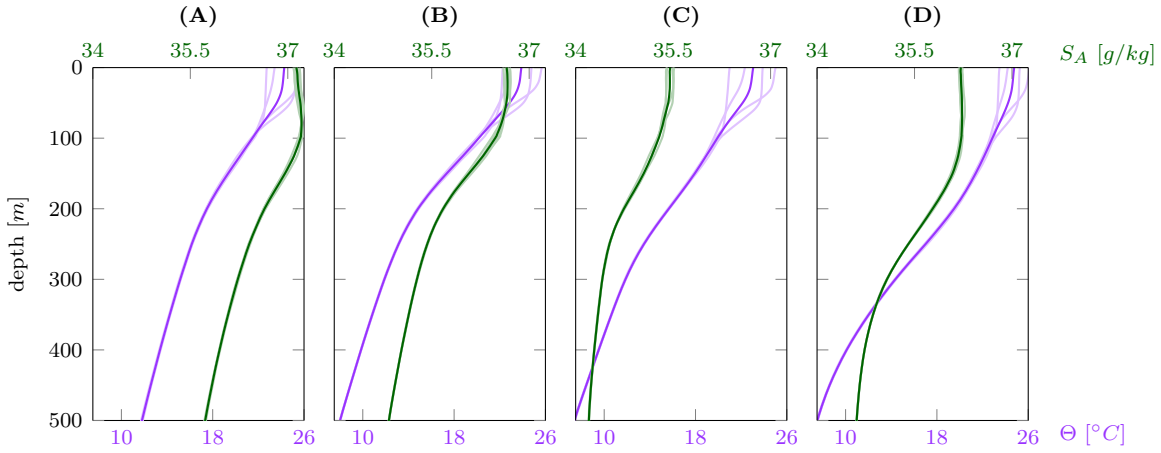

Figure 4: Annual mean depth profiles for conservative temperature (violet) and absolute salinity (green), for NAG (A), SAG (B), NPG (C), and SPG (D), with seasonal variation (light colors). Data taken from Boyer *et al.* (2018).

From Figure 4 it can be seen that, especially for the salinity profiles, the seasonal variability is very small. The temperature profiles show a slightly larger seasonal variability with greater surface temperatures in the local summer and autumn. The rest of the studies described in this work will be based on the mean profiles shown in Figure 4. It should be kept in mind that they do not represent the most ideal conditions for SUP-based AU, but rather the average conditions of all regions which might be of practical interest, based on the annual mean salinity differences from Figure 3.

3.3 Single pipe and counterflow pipe

In this section, results for a simple single SUP are compared to those of a counterflow SUP. The annual mean depth profiles from Section 3.2 are used along with the reference geometries and calculation setups from Section 3.1.

Figure 5 shows the results of this study. Here, the upwelling rates for both pipe setups under the different ocean conditions are depicted. Results from both models are shown. Additionally results from calculations of a single SUP including the surrounding ocean are given.

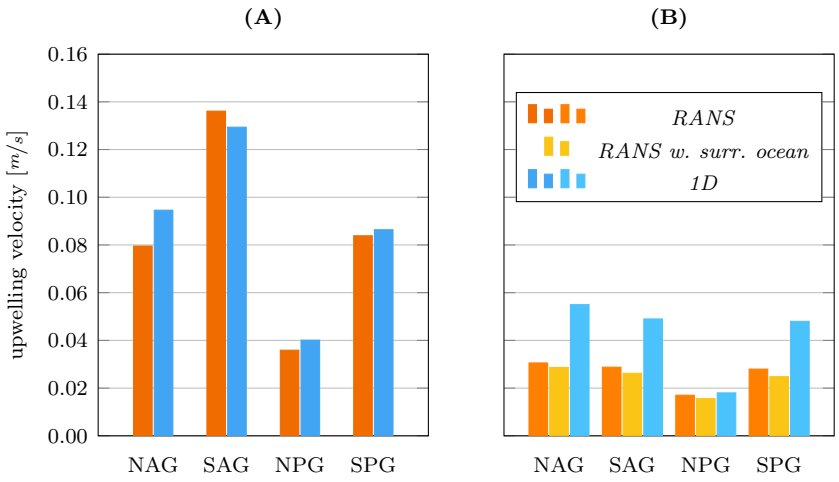

Figure 5: Upwelling velocities obtained by the counterflow- (A) and single pipe (B) setup, for the depth profiles described in Section 3.2, as predicted by the RANS (red, orange) and one-dimensional (blue, light blue) model.

From Figure 5 it can clearly be seen that the counterflow setup performs much better than the simple setup under all conditions. While it has to be taken into account that the relative performance of the two SUP concepts might change when both pipe geometries are thoroughly optimized, the magnitude of the differences observed in Figure 5 can be seen as an indication towards a clear superiority of the counterflow SUP design. Conceptually this is explained by the more efficient heat transfer of the counterflow setup. Figure 6 shows temperature profiles, from the RANS and one-dimensional calculations, for the SAG case. Here, it can be seen that, while for the counterflow SUP the temperature difference across the pipe wall ($\Delta_r\Theta$) is almost constant along the pipe, for the single SUP the temperature difference varies strongly in the axial direction. Efficient heat transfer is thus only possible over a smaller portion of the length of the single SUP.

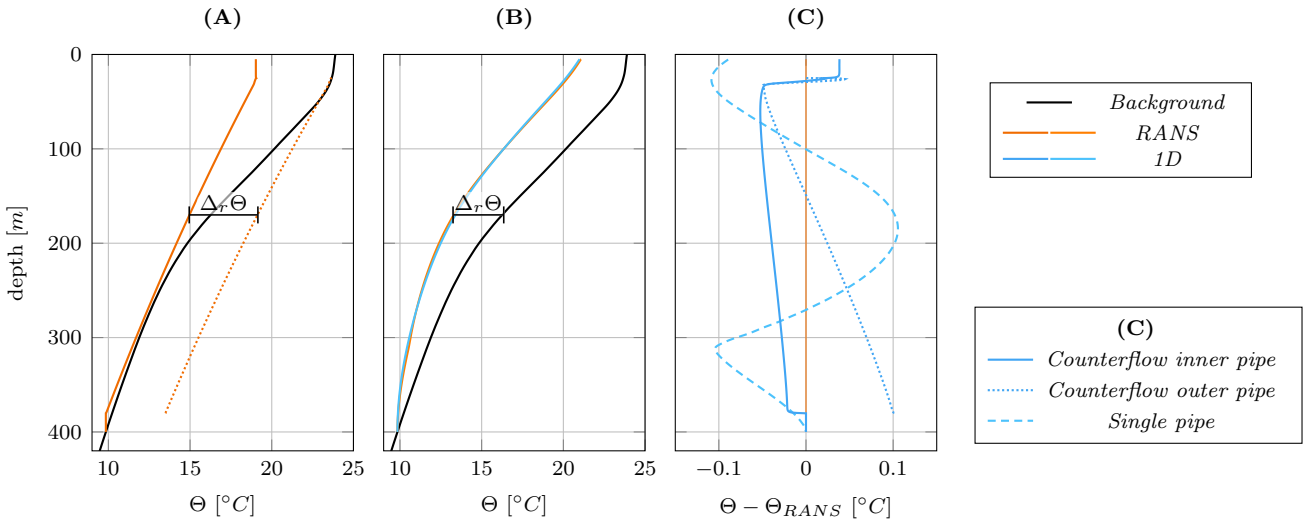

Figure 6: Temperature depth profiles in the Stommel-pipe system (colored) and the background ocean (black), from the RANS (orange) and one-dimensional (blue) calculations, for the SAG case. Results for a counterflow SUP (A) and a single SUP (B) are shown. A comparison of the temperature differences between the one-dimensional- and RANS results is shown in (C).

As can be seen in Figures 5 and 6, the differences between the results of both models are very small in the counterflow cases. Although the differences for the single pipe are non negligible for some cases, it will be shown later (Section 3.4) that the overall agreement is still reasonably good. In the absence of experimental data for validation, this is seen as an indication that both models can be used to predict SUP performance in different ocean regions with confidence. As clearly visible from Figure 6 (C), the difference in calculated temperature (between the one-dimensional and RANS results) shows steep changes for the couterflow case where the heat transfering region begins and ends. This is presumably caused by to the changing flow profile in the RANS calculations due to the unheated inlet and outlet region - an effect that is not accounted for in the one-dimensional calculations. It can be observed, that the heat transfer is slightly underestimated for this case, leading to a minor difference in absolute temperature. As shown in Figure 5, the difference in velocity for the single pipe case between the one-dimensional and the RANS solution is significant, thereby differences in predicted temperature are not surprising, although being mostly within 0.1 °C.

3.4 Geometric Variation Study

The study presented in Section 3.3 has shown that the results from both models are in reasonable agreement. However, the computational effort needed to obtain these results varies by orders of magnitude between the two models, making the one-dimensional model far more suitable for large parametric studies. This capability will be demonstrated in this section by performing a simple study on the pipe diameter. Starting from the reference geometries for the single- and counterflow SUP from Section 3.1, the diameter of the (inner) pipe is systematically varied from 0.025 m to 0.5 m in 19 steps. For the counterflow SUP, the outer pipe diameter is determined from the constant cross sectional flow area ratio of inner and outer pipe, which has a value of 0.5. The SAG profile from Section 3.2 is used as a background ocean profile for this study. Figure 7 shows the variation of the upwelling flow velocity and flow rate over the changing diameter for both the single- and counterflow SUP. Additionally the density difference between the upwelled DOW leaving the pipe at the top and the surrounding water is shown. Here, a positive value indicates that the upwelled DOW has a lower density compared to the surrounding water when leaving the system, while a negative value indicates a higher density and thus a negative buoyancy of the upwelled DOW.

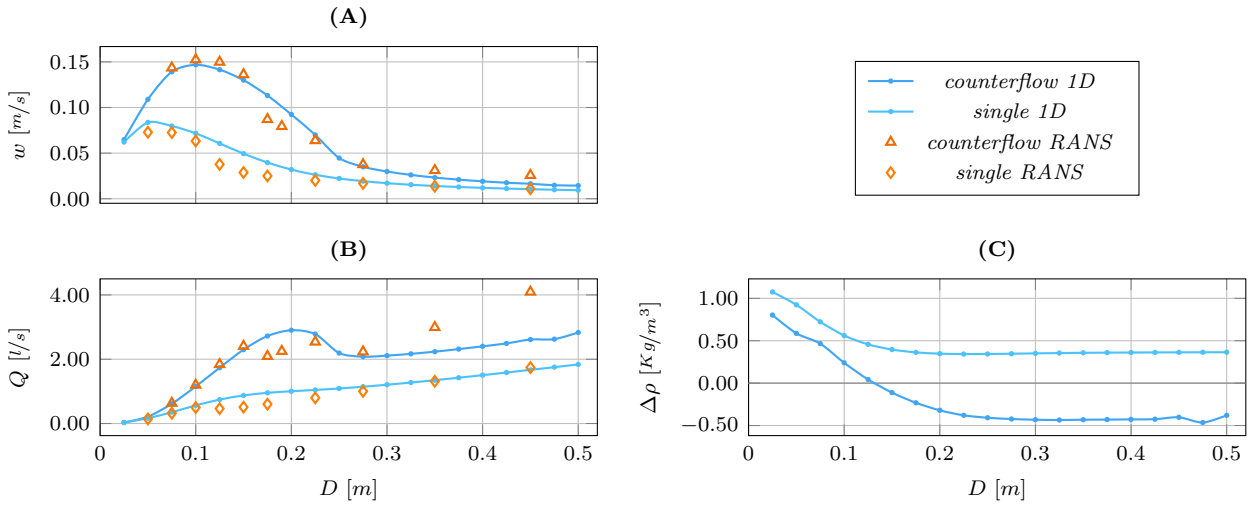

Figure 7: Pipe diameter study: Upwelling velocity (A), flow rate (B) and density difference at outlet (C) over (inner) pipe diameter of a counterflow SUP (orange) and a single SUP (blue).

It can be seen from Figure 7 (A) and (B) that the predicted flow rates of both methods show a good overall agreement, further underlining the capability of the one-dimensional method. Obvious deviations can be observed for diameters in the range of 0.10 m to 0.25 m, which might explain the differences for the single SUP observed in Figure 5 (B). Careful inspection of the RANS results indicated that those deviations could be explained by insufficient reproduction of mixed convection in the one-dimensional method. Deviations can also be observed for the counterflow setup at high diameters. Due to the small velocity differences in absolute terms, this effect was not further studied. It can be seen from Figure 7 (B) that the flow rate Q increases monotonically with the pipe diameter for the single pipe system, while the counterflow system shows an early peak at ≈ 0.2 m. The flow velocity w (Figure 7 (A)) increases with decreasing diameter until a certain diameter (0.1 m counterflow, 0.05 m single) below which w decreases rapidly with a further decrease in pipe diameter. This decrease of the velocity for small diameters can be attributed to laminarization of the flow, which drastically decreases the heat transfer efficiency. Generally, the flow rates for the counterflow SUP are higher than those of the single SUP, further supporting the superiority of the counterflow concept. Please note that the results of Figure 7 where obtained for a single ocean profile and will look differently for other boundary conditions.

While for general applications of AU it is usually sufficient that the upwelled DOW remains in the oceans mixed surface layer, further rise to the water surface marks an essential requirement for surface bound macroalgae farming. As can be seen from Figure 7 (C) the DOW is generally positively buoyant when when leaving the system, in the single SUP case. For the counterflow SUP, the water is only positively buoyant if small diameter pipes are used. For many of the counterflow setups, the DOW will thus have the tendency to sink back down after leaving the pipe, even though it has been heated to some extent. This clearly depicts that the re-sinking problem of Kirke (2003) is not generally circumvented by using the salt fountain principle for AU. The buoyancy of the upwelled DOW leaving the system varies greatly, based on the pipe design and and also the local ocean depth profiles (i. e. Θ and S_A). For instance, Maruyama *et al.* (2004) found the DOW upwelled by their single SUP to be negatively buoyant because the surface waters in their deployment region were of relatively low salinity. The higher re-sinking risk as consequence of a higher flow rate is a clear disadvantage of counterflow SUPs and stands against the advantages of these systems, which were previously described. In many cases, extending the upwelling pipe with a horizontal section at the top, will likely be sufficient to overcome this disadvantage at the cost of a moderately increased frictional flow resistance. Such an extension has not been studied to date, however, due to the high turbulence and the action of waves and currents in the surface ocean, it can be expected to have a high heat transfer efficiency. Finally, it should be noted that a high salinity difference between the DOW and the surface water is crucial for obtaining a positive buoyancy of the DOW. For the single SUP case presented in Figure 7 (C) positive buoyancy was obtained due to the salinity effect, despite the upwelled DOW being up to 3.3 °C colder than the surrounding surface water. If the DOW does not have a lower salinity than the surface water, as in the case of Maruyama *et al.* (2004), positive buoyancy of the upwelled DOW can obviously not be obtained with the salt fountain principle.

3.5 Shell-And-Tube Type SUP Systems

The possibility of arranging multiple inner pipes in a larger outer shell has already been pointed out by Johnson and Decicco (1983). Here, only counterflow SUPs with a single inner pipe have been studied so far. For these, the outer pipe takes the simple shape of a cylinder annulus. The complex geometries of shell-and-tube type SUPs can ideally be studied using the RANS model. For this purpose, two shell-and-tube setups with 7 and 19 inner pipes are studied, in addition to a counterflow setup with

a single inner pipe. The geometries follow the reference geometry defined in Section 3.1 with respect to inner pipe diameter, pipe lengths and material thickness. The shell diameter is determined from the constant cross sectional flow area ratio of 0.5. For the shell-and-tube setups, the inner pipes are arranged evenly on concentric circles whose diameters were optimized to provide an even spacing among the pipes and with respect to the outer shell.[4] The symmetry of the setups was used, such that only a 60° section of each SUP system had to be resolved. The resulting computational meshes for the 1, 7 and 19 pipe case contained about 660, 3660 and 9400 cells in the horizontal plane and 1000 cells over the pipe length. Figure 8 shows cross sections of all three meshes, as well as velocity profiles at the medium depth, obtained from the RANS calculations.

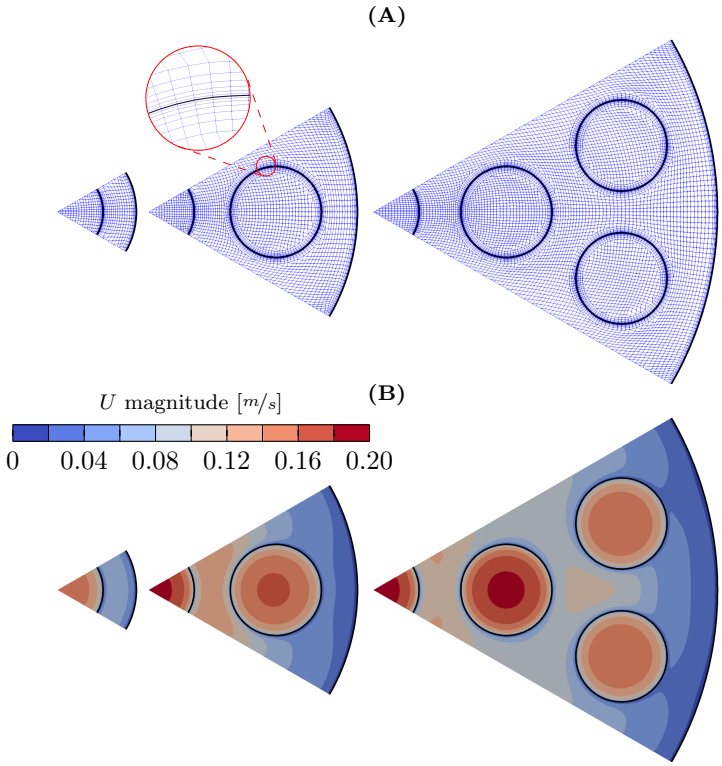

Figure 8: Shell-and-tube type SUP study: Cross sections of computational meshes with 1, 7 and 19 inner pipes (A) as well as predicted velocity magnitude over the cross sections (B).

From the velocity profiles shown in Figure 8 (B) it can be seen that upwelling velocity is generally highest in the innermost pipe and decreases in the outer rows. Equally, the downwelling velocity is highest in the center of the shell and decreases towards the sides. The decrease of the downwelling velocities leads to a less efficient heat transfer in the outer upwelling pipes and thus explains the lower upwelling velocities in these pipes. Generally, the installation of baffles, as typically seen in shell-and-tube heat exchanges, might help to even out the performance of the different inner pipes in a shell-and-tube type SUP, even though this would clearly impair the shell-side flow and might also be problematic from a technical point of view.

Figure 9 provides a more detailed picture of the scaling of the upwelling velocities with the number of inner pipes. Here, the average upwelling velocity over all pipes and the average downwelling velocity

[4]For the 7 inner pipe case, the pipes were arranged on a 0.419 m diameter circle. The shell diameter was 0.687 m. For the 19 inner pipe case, a 0.437 m and a 0.845 m diameter circle were used for pipe arrangement, while the shell diameter was 1.132 m.

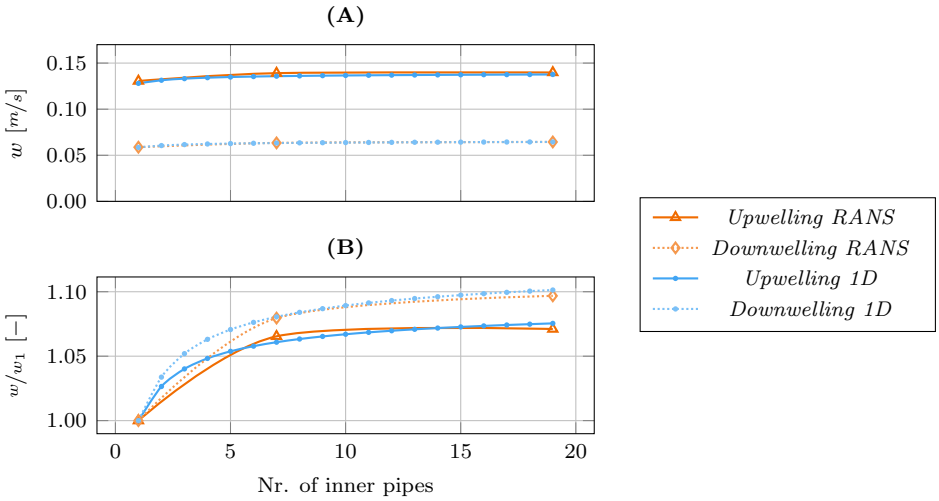

Figure 9: Shell-and-tube type SUP study: Variation of average up- (solid) and downwelling (dotted) velocities (RANS: orange, one-dimensional: blue) over the number of inner pipes in the system as absolute- (A) and normalized (B) values.

in the shell are plotted over the number of pipes in the shell-and-tube SUP. For comparison results from the one-dimensional method are shown. Here the scaling was done as described in Section 2.2. Figure 9 shows that the average up- and downwelling velocities are only weakly influenced by the overall SUP system size. A slight increase of both, up- and downwelling velocities is observed, which appears to tend towards a finite limit for large numbers of inner pipes For the cases presented here, the maximum increase is about 10 % for downwelling and 7 % for upwelling. Again, the results of the one-dimensional method are in good agreement with the RANS results. The results suggest that the scaling of shell-and-tube type SUPs is very well reproduced by the one-dimensional method. While the inner pipe dimensions, as well as inner-to-outer-pipe cross-sectional flow area ratio, were kept constant throughout this study, the shell-side hydraulic diameter D_{ho} inevitably increases with an increasing number of inner pipes and varies by a factor of about 2 between the presented setups. For the one-dimensional calculations, the change in D_{ho} is in fact the only parameter change in this study. The shell-side hydraulic diameter thus seems to be an important quantity for understanding and optimizing the performance of shell-and-tube type SUPs. It should be noted that the scaling of the average up- and downwelling velocities observed in Figure 9 might depend significantly on other geometrical parameters of the SUP and cannot be seen as universal. For instance, it was noted during the RANS studies that the results depend to some extent on the arrangement of the inner pipes in the shell. The results of this study suggest that that the hydraulic diameter scaling of the one-dimensional method resembles the idealized situation of evenly spaced inner pipes, which cannot always be achieved in reality. To what extent uneven pipe spacing influences the results remains to be studied.

4. CONCLUSIONS

Two numerical models for SUP systems have been proposed in this work. Both models have been described in detail. Results from both models have been compared for a range of variations in ocean depth profiles and SUP geometries. Finally, some studies of shell-and-tube type SUPs were presented, showing the upscaling potential for practical use cases.

In all calculations presented in this work, significant upwelling through the SUP principle was found. Counterflow SUPs generally perform superior to comparable single SUPs. However, the higher flow

rates of these systems result in a lower probability of the DOW leaving the system buoyant with respect to its surroundings at the surface. Additional measures may thus be necessary for counterflow SUPs to avoid re-sinking problem of conventional AU pumps. Shell-and-tube type systems where found to show a slight increase in upwelling velocity for increasing number of inner pipes. These systems thus offer high potential for scaling to desired volumetric flow rates for practical applications.

The results generally show very good agreement between both of the proposed models. In the absence of suitable experimental data for validation, the agreement of the presented models is seen as an indication towards a good reliability of both models in predicting the performance of different types of SUP systems with different geometries in various ocean regions.

In the thrive to enhance the technology readiness level of AU-based CDR, reliable model predictions for the potential of various technical approaches are essential. Such general assessments require larger sets of technical parameters and ocean conditions to be studied. To quantify the CDR potential, consideration must be extended beyond the mere SUP system to include environmental influences as well as biogeochemical responses and feedback. The methods presented in this work provide a versatile and reliable basis for these efforts.

The following future work is recommended:

- Parametric studies on a wide range of technical parameters should be performed to provide a more general overview of the performance and potential of SUP systems for AU.
- A larger set of ocean conditions should be studied and potential regions for deployment and prototype testing should be identified.
- Practical use scenarios for SUP-based AU should be defined and studied, including corresponding environmental effects (e. g. currents and waves) as well as biogeochemical responses and feedback.
- Careful validation of both methods presented in this work against experimental data is needed to further prove their predictive capabilities.
- Since sufficient experimental data is not currently available, experiments of the salt fountain phenomenon have to be performed on both lab- and full-scale.

ACKNOWLEDGEMENTS

This study was funded by the German *Federal Ministry of Education and Research* (Bundesministerium für Bildung und Forschung, BMBF) in the framework of the the *Test-ArtUp* project, which is part of the *CDRmare* research mission lead by the *German Marine Research Alliance* (Deutsche Allianz Meeresforschung, DAM), under Grant Agreement No. 03F0897B. This study was further funded by the German *Federal Agency for Disruptive Innovations* (Bundesagentur für Sprunginnovationen, SPRIND GmbH) in the framework of the *C-CAUSE* project within the *Carbon-To-Value* challenge.

AUTHOR'S CONTRIBUTION

J. Ke. developed and implemented the numerical RANS method and performed the RANS calculations. J. Ke. and J. M. developed the one-dimensional method and analyzed the results under the scientific and technical supervision of U. R., J. Kr. and K. G.. J. Ke. and J. M. wrote the manuscript with input from all authors.

REFERENCES

Boyer, T. P., Baranova, O. K., Coleman, C., Garcia, H. E., Grodsky, A., Locarnini, R. A., *et al.* (2018). *World Ocean Database 2018*. Tech. rep., National Centers for Environmental Information Ocean Climate Laboratory, Silver Spring, MD, USA

Burg, K., Haf, H., Wille, F., and Meister, A. (2013). *Höhere Mathematik für Ingenieure: Band III: Gewöhnliche Differentialgleichungen, Distributionen, Integraltransformationen* (Wiesbaden: Springer Fachmedien Wiesbaden). doi:10.1007/978-3-8348-2334-2

Cebeci, T. (1974). Laminar-Free-Convective-Heat Transfer from the Outer Surface of a Vertical Slender Circular Cylinder. In *Proceeding of International Heat Transfer Conference 5* (Tokyo, Japan: Begellhouse), 15–19. doi:10.1615/IHTC5.2830

Churchill, S. W. and Chu, H. H. S. (1975). Correlating Equations for Laminar and Turbulent Free Convection from a Vertical Plate. *International Journal of Heat and Mass Transfer* 18, 1323–1329. doi:10.1016/0017-9310(75)90243-4

Fan, W., Pan, Y., Liu, C. C., Wiltshire, J. C., Chen-Tung, A. C., and Chen, Y. (2015). Hydrodynamic Design of Deep Ocean Water Discharge for the Creation of a Nutrient-rich Plume in the South China Sea. *Ocean Engineering* 108, 356–368. doi:10.1016/j.oceaneng.2015.08.006

GESAMP (2019). High Level Review of a Wide Range of Proposed Marine Geoengineering Techniques. *GESAMP Reports and Studies* 98, 144

Gnielinski, V. (2018a). Wärmeübertragung bei erzwungener Konvektion: Durchströmte Rohre. In *VDI-Wärmeatlas*, eds. P. Stephan, D. Mewes, S. Kabelac, M. Kind, K. Schaber, and T. Wetzel (Berlin, Heidelberg: Springer Berlin Heidelberg). 1–9. doi:10.1007/978-3-662-52991-1_42-1

Gnielinski, V. (2018b). Wärmeübertragung bei erzwungener Konvektion: Konzentrischer Ringspalt und ebener Spalt. In *VDI-Wärmeatlas*, eds. P. Stephan, D. Mewes, S. Kabelac, M. Kind, K. Schaber, and T. Wetzel (Berlin, Heidelberg: Springer Berlin Heidelberg). 1–9. doi:10.1007/978-3-662-52991-1_43-1

Groves, G. W. (1958). Flow Estimate for the Perpetual Salt Fountain. *Deep Sea Research (1953)* 5, 209–214. doi:10.1016/0146-6313(58)90013-3

Hinman, K. G. (1966). *Flow Velocity Calculations for a "Perpetual Salt Fountain"*. Master's thesis, United States Naval Postgraduate School

Incropera, F. P., DeWitt, D. P., Bergman, T. L., and Lavine, A. S. (eds.) (2013). *Principles of Heat and Mass Transfer* (Hoboken, NJ: Wiley), 7. ed., international student version edn.

IOC, SCOR, and IAPSO (2010). The International Thermodynamic Equation of Seawater - 2010: Calculation and Use of Thermodynamic Properties. *Intergovernmental Oceanographic Commission, Manuals and Guides* 56, 196

IPCC (2021). *Climate Change 2021: The Physical Science Basis. Contribution of Working Group I to the Sixth Assessment Report of the Intergovernmental Panel on Climate Change*, vol. In Press (Cambridge, United Kingdom and New York, NY, USA: Cambridge University Press). doi:10.1017/9781009157896

Jamieson, D. and Tudhope, J. (1970). Physical Properties of Sea Water Solutions: Thermal Conductivity. *Desalination* 8, 393–401. doi:10.1016/S0011-9164(00)80240-4

Jasak, H., Weller, H., and Gosman, A. (1999). High Resolution NVD Differencing Scheme for Arbitrarily Unstructured Meshes. *International Journal for Numerical Methods in Fluids* 31, 431–449. doi:10.1002/(sici)1097-0363(19990930)31:2⟨431::aid-fld884⟩3.0.co;2-t

Johnson, D. H. and Decicco, J. (1983). *Artificial Upwelling Driven by Salinity Differences in the Ocean*. Tech. rep., Solar Energy Research Inst., Golden, CO (USA)

Kemper, J., Riebesell, U., and Graf, K. (2022). Numerical Flow Modeling of Artificial Ocean Upwelling. *Frontiers in Marine Science* 8. doi:10.3389/fmars.2021.804875

Kirke, B. (2003). Enhancing Fish Stocks with Wave-powered Artificial Upwelling. *Ocean & Coastal Management* 46, 901–915. doi:10.1016/s0964-5691(03)00067-x

Liang, N.-K. and Peng, H.-K. (2005). A Study of Air-lift Artificial Upwelling. *Ocean Engineering* 32, 731–745. doi:10.1016/j.oceaneng.2004.10.011

Lovelock, J. E. and Rapley, C. G. (2007). Ocean Pipes Could Help the Earth to Cure Itself. *Nature* 449, 403–403. doi:10.1038/449403a

Maruyama, S., Tsubaki, K., Taira, K., and Sakai, S. (2004). Artificial Upwelling of Deep Seawater Using the Perpetual Salt Fountain for Cultivation of Ocean Desert. *Journal of Oceanography* 60, 563–568. doi:10.1023/b:joce.0000038349.56399.09

Maruyama, S., Yabuki, T., Sato, T., Tsubaki, K., Komiya, A., Watanabe, M., *et al.* (2011). Evidences of Increasing Primary Production in the Ocean by Stommel's Perpetual Salt Fountain. *Deep Sea Research Part I: Oceanographic Research Papers* 58, 567–574. doi:10.1016/j.dsr.2011.02.012

McDougall, T. J. (2003). Potential Enthalpy: A Conservative Oceanic Variable for Evaluating Heat Content and Heat Fluxes. *Journal of Physical Oceanography* 33, 945–963. doi:10.1175/1520-0485(2003)033⟨0945:peacov⟩2.0.co;2

Menter, F. R. (1994). Two-equation Eddy-viscosity Turbulence Models for Engineering Applications. *AIAA Journal* 32, 1598–1605. doi:10.2514/3.12149

Menter, F. R., Kuntz, M., and Langtry, R. (2003). Ten Years of Industrial Experience with the SST Turbulence Model. *Turbulence, heat and mass transfer* 4, 625–632

Morrison, F. A. (2013). *An Introduction to Fluid Mechanics* (Cambridge University Press), 1 edn. doi:10.1017/CBO9781139047463

Popiel, C., Wojtkowiak, J., and Bober, K. (2007). Laminar Free Convective Heat Transfer from Isothermal Vertical Slender Cylinder. *Experimental Thermal and Fluid Science* 32, 607–613. doi:10.1016/j.expthermflusci.2007.07.003

Sato, T., Maruyama, S., Komiya, A., and Tsubaki, K. (2007). Numerical Simulation of Upwelling Flow in Pipe Generated by Perpetual Salt Fountain. In *Proceedings of the 16th Australasian Fluid Mechanics Conference, Crown Plaza, Gold Coast, Australia*. 394–397

Shah, R. K. and Sekulić, D. P. (2003). *Fundamentals of Heat Exchanger Design* (Hoboken, NJ: John Wiley & Sons)

Stommel, H., Arons, A. B., and Blanchard, D. (1956). An Oceanographical Curiosity: The Perpetual Salt Fountain. *Deep Sea Research (1953)* 3, 152–153. doi:10.1016/0146-6313(56)90095-8

Thess, A. and Kaiser, R. (2018a). Wärmeübertragung bei freier Konvektion: Außenströmungen. In *Handbuch Vakuumtechnik*, ed. K. Jousten (Wiesbaden: Springer Fachmedien Wiesbaden). 1–10. doi:10.1007/978-3-662-52991-1_38-1. Series Title: Springer Reference Technik

Thess, A. and Kaiser, R. (2018b). Wärmeübertragung bei freier Konvektion: Innenströmungen. In *Handbuch Vakuumtechnik*, ed. K. Jousten (Wiesbaden: Springer Fachmedien Wiesbaden). 1–11. doi:10.1007/978-3-662-52991-1_39-1. Series Title: Springer Reference Technik

Tsubaki, K., Maruyama, S., Komiya, A., and Mitsugashira, H. (2007). Continuous Measurement of an Artificial Upwelling of Deep Sea Water Induced by the Perpetual Salt Fountain. *Deep Sea Research Part I: Oceanographic Research Papers* 54, 75–84. doi:10.1016/j.dsr.2006.10.002

Wu, J., Keller, D. P., and Oschlies, A. (2023). Carbon Dioxide Removal Via Macroalgae Open-ocean Mariculture and Sinking: An Earth System Modeling Study. *Earth System Dynamics* 14, 185–221. doi:10.5194/esd-14-185-2023

Young, W. R. (2010). Dynamic Enthalpy, Conservative Temperature, and the Seawater Boussinesq Approximation. *Journal of Physical Oceanography* 40, 394–400. doi:10.1175/2009jpo4294.1

Zhang, X., Maruyama, S., Sakai, S., Tsubaki, K., and Behnia, M. (2004). Flow Prediction in Upwelling Deep Seawater—the Perpetual Salt Fountain. *Deep Sea Research Part I: Oceanographic Research Papers* 51, 1145–1157. doi:10.1016/j.dsr.2004.03.010

Zhang, X., Maruyama, S., Tsubaki, K., Sakai, S., and Behnia, M. (2006). Mechanism for Enhanced Diffusivity in the Deep-Sea Perpetual Salt Fountain. *Journal of Oceanography* 62, 133–142. doi:10.1007/s10872-006-0039-5